SNR Coverage Probability Analysis of RIS-Aided Communication Systems

Zhuangzhuang Cui, *Student Member, IEEE,* Ke Guan, *Senior Member, IEEE,*
Jiayi Zhang, *Senior Member, IEEE,* and Zhangdui Zhong, *Senior Member, IEEE*

***Abstract*—The reconfigurable intelligent surface (RIS) technique has received many interests, thanks to its advantages of low cost, easy deployment, and high controllability. It is acknowledged that the RIS can significantly improve the quality of signal transmission, especially in the line-of-sight-blocked scenarios. Therefore, it is critical to analyze the corresponding signal-to-noise ratio (SNR) coverage probability of RIS-aided communication systems. In this correspondence, we consider many practical issues to analyze the SNR coverage probability. We employ the realistic path loss model and Rayleigh fading model as large-scale and small-scale channel models, respectively. Meanwhile, we take the number and size of the RIS elements, as well as the placement of the RIS plane into considerations. We first derive the exact closed-form SNR coverage probability for a single element. Afterward, with the moment matching method, a highly accurate approximation of SNR coverage probability is formulated as the ratio of the upper incomplete Gamma function and Gamma function, allowing an arbitrary number of elements in the RIS. Finally, we comprehensively evaluate the impacts of essential factors on the SNR coverage probability, such as the number and size of the element, the coefficients of fading channel, and the angles of incidence and RIS plane. Overall, this work provides a succinct and general expression of SNR coverage probability, which can be helpful in the performance evaluation and practical implementation of the RIS.**

***Index Terms*—Coverage probability, fading channel, reconfigurable intelligent surface, Rayleigh fading, signal-to-noise ratio.**

I. Introduction

THE reconfigurable intelligent surface (RIS) has drawn great attention in both academia and industry since it is capable of smartly designing the radio environment by adjusting the phase and magnitude of the incoming wave operated by a central controller, and thereby improving the signal quality [1]. In the RIS-aided communication system, the RIS is expected to *passively reflect* transmitted signals, and then the resultant signal can be received in any desired direction. Thus, the RIS technology can remedy the defect of limited coverage in millimeter-wave communications [2]. Moreover, in the scenario where the line-of-sight (LOS) path is obstructed, the RIS can significantly enhance the received power strength through the constructive superposition of impinging waves from each surface in the RIS. It is worth mentioning that the RIS does not need radio frequency (RF) links, which essentially differs from the traditional relay technology. In brief, the advantages of low-cost, multi-use, and easy-to-deployment have impelled many researchers to focus on the RIS technique [3].

At the initial stage of the RIS study, the high energy efficiency in wireless communications is pursued by the assistance of RIS since the RIS is more superior to the relay technology in energy consumption [4], [5]. Moreover, as an advanced evolution of RIS, the passive holographic multiple-input multiple-output surface (HMIMOS) has been proposed as a key enabling technology for the physical layer of the sixth generation (6G) wireless networks [6], [7]. For terahertz communications, the RIS plays an increasingly important role in remedying the huge path loss by deploying the RIS with a great number of surfaces, thanks to small wavelengths in terahertz bands [8]. Besides, many works are also focusing on the optimal phase shift or beamforming design of the RIS [9].

In terms of the performance analysis of RIS-assisted communications, there are abundant works that have sprung in recent years [10]-[12]. The authors in [10] analyzed the essential performances, i.e., the ergodic channel capacity and outage probability, under Rician fading channels for both transmitter-to-RIS (TS) and RIS-to-receiver (SR) links and Rayleigh fading for the transmitter-to-receiver (TR) link. Moreover, by employing the central limit theorem (CLT) that assumes the number of surfaces in RIS is sufficiently large, the approximate outage probability is obtained. In [11], consider Rayleigh fading for both TS and SR links in a LOS-blocked scenario, the received signal-to-noise ratio (SNR) is tightly approximated by a non-central chi-squared distribution with a single degree-of-freedom (DoF). Thus, the outage probability is readily obtained. In [12], under Rayleigh fading for both TS and SR links and Rician fading for the TR link, the ergodic rate is analyzed and optimized in terms of the phase shift of RIS, considering the interfering base stations.

We can find that the fading channel plays an essential role in the performance analysis. The distributions of small-scale fading including Rayleigh, Rician, and Nakagami-*m* [13] are involved in existing works. However, the large-scale fading is simply modeled as a function of link distance, which overlooks the physical characteristics of the RIS. After determining the fading channels, the key is to derive the distribution of SNR for the analysis [14]. The popular method is based on the CLT that assumes the number of surfaces $N \gg 1$ [15], [16]. Then, the resultant amplitude of fading channels is approximated as a Gaussian random variable (RV), which becomes tractable. Nevertheless, the assumption of an extremely large number of surfaces may not be in line with the actual situation.

In this work, we aim to analyze the SNR coverage probability for RIS-assisted single-input single-output (SISO) commu-

This work was supported by Key-Area Research and Development Program of Guangdong Province, China (2019B010157001), the NSFC under Grant (61771036, 61901029, U1834210, and 61725101), the State Key Laboratory of Rail Traffic Control and Safety (Contract No. RCS2020ZZ005). (*Corresponding authors: Ke Guan, Jiayi Zhang*).

The authors are with the State Key Laboratory of Rail Traffic Control and Safety, Beijing Jiaotong University, Beijing, 100044 China. (E-mail: {cuizhuangzhuang, kguan, zhangjiayi, zhdzhong}@bjtu.edu.cn.)

nications. The main reasons are as follows. The SNR coverage probability is one of the essential metrics in the performance analysis of communication systems. It can not only evaluate the quality of signal transmission but also provide insights into the practical deployment of communication systems. More specifically, the coverage probability is the complementary cumulative distribution function (CCDF) of SNR at the receiver. Recent works use the same metric in the performance analysis for RIS-aided communication systems [17], [18]. However, there remain some deficiencies that need to be made up. As an example, both works neglected the impact of the physical size of RIS on the large-scale fading such as path loss. Inspired by the above review, technical motivations can be summarized as follows. First, the performance analysis of RIS-aided communication system needs to consider a more practical channel model that can take the *physical characteristics of the RIS* into account [19]. Then, the amplitude of the *composite fading channel* is represented as the sum of the product of two RVs following specific distribution, which poses a challenge to determine the distribution of SNR. Last but not least, due to many factors, such as the physical size of RIS and channel conditions that can affect SNR coverage probability, an elaborate and comprehensive analysis is urgently needed.

Consider the above deficiencies and challenges, we use a more realistic channel model and allow an arbitrary number of elements in the SNR coverage probability analysis. The main contributions are summarized as follows: (i) We employ a *realistic path loss model* that takes the physical size of RIS and the effective angle of incidence into account, which allows us to quantify their impacts on the SNR coverage probability. (ii) For a *single element*, we determine the distribution of resultant channel gain under Rayleigh fading, and then the exact closed-form SNR coverage probability is obtained. (iii) For *multiple elements*, we utilize the Gamma distribution to approximate the distribution of resultant channel gain by the moment matching method and then derive a tractable and accurate expression of SNR coverage probability. (iv) We comprehensively analyze many factors that can influence the SNR coverage probability by numerous simulations.

II. System Model

We consider a general RIS-aided communication system, where the direct link is nonexistent due to blockage, as shown in Fig. 1(a). As a result, the RIS with the size of $u \times w$ and the number of N metallic elements reflects the wave from one single-antenna source (S) to one single-antenna destination (D). Note that u and w are the aggregate length and width of all elements in the RIS, respectively. Besides, the distances of TS and SR links are denoted as d_s and d_r, respectively. It is worth noting that we consider the far-field transmission for the transceivers, which means that $d_s, d_r \geq \frac{2(\max\{u,w\})^2}{\lambda}$ where λ is the wavelength. Fig. 1(b) shows that the angle of incidence is denoted as $\theta_i = \langle \mathbf{n_O}, \mathbf{n_I} \rangle$, that is the angle between the incident direction of the incoming wave and the normal direction of the vertically placed RIS plane. To consider a more general case that includes the placement of the RIS plane, we denote the rotation angle of the RIS plane as $\theta_R = \langle \mathbf{n_O}, \mathbf{n_R} \rangle$. Note that the angle of θ_R is 0° when the RIS plane is vertically straight.

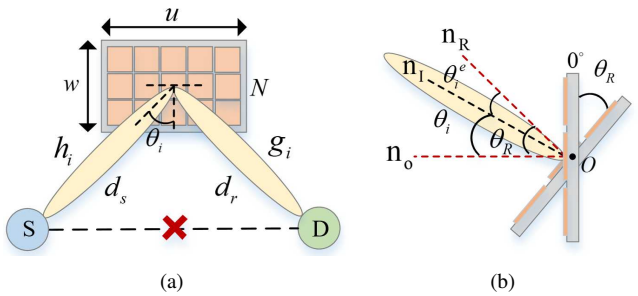

(a) (b)

Fig. 1. System model: (a) an RIS-aided communication system with N elements, (b) an illustration of the rotation of RIS plane with an angle of θ_R.

A. Channel Model

Prior works focus on modeling the path loss for the RIS-assisted communications [21], [22]. For instance, in [21], the authors proposed the free space path loss models for both the near-field and far-field conditions. Moreover, experimental measurements were conducted to verify these models. In this work, our objective is to introduce the size of the RIS and the angle of incidence into the path loss, thus, a realistic large-scale path loss model in the far-field is used as [22]

$$P_l(d_s, d_r, \theta_i^e) = \frac{G_s G_r}{(4\pi)^2} \left(\frac{uw}{d_s d_r}\right)^2 \cos(\theta_i^e), \tag{1}$$

where G_s and G_r are the antenna gains of transmitter and receiver, respectively. In addition, θ_i^e represents the effective incident angle that is determined as $|\theta_i - \theta_R|$ according to the geometric relationship.

Then, we denote the amplitudes of small-scale fading of TS and SR links as α_i and β_i, where i is the index of the element in the RIS. They both follow Rayleigh distribution as [15], with probability density function (PDF) given by

$$f_\alpha(\alpha) = \frac{\alpha}{\sigma^2} \exp\left(-\frac{\alpha^2}{2\sigma^2}\right), \tag{2}$$

where σ represents the fading coefficient of the channel.

B. Signal-to-Noise Ratio

Assuming that the channels of TS and SR links experience the quasi-static Rayleigh fading without interference, the received signal can be expressed as

$$y = \sqrt{P_s P_l} \left[\sum_{i=1}^{N} h_i \chi_i g_i\right] x + n_0, \tag{3}$$

where x is the transmit signal with the power of P_s and $\chi_i = \varrho_i(\phi_i) e^{j\phi_i}$ is the reflection coefficient produced by the ith element, with $\varrho_i(\phi_i) = 1$ for the ideal condition ($\forall i = 1, 2, ..., N$). Note that $h_i = \alpha_i e^{-j\vartheta_i}$ and $g_i = \beta_i e^{-j\varphi_i}$ are channel gains. We assume that the channel state information (CSI) of all channels is perfectly known [16]. Moreover, n_0 is the additive white Gaussian noise following $\mathcal{N}(0, \sigma_n^2)$. Then, the received SNR can be expressed as

$$\gamma = \frac{\left|\sum_{i=1}^{N} \alpha_i \beta_i e^{j(\phi_i - \vartheta_i - \varphi_i)}\right|^2 P_s G_s G_r (uw \cos(\theta_i^e))^2}{(4\pi \sigma_n d_s d_r)^2}. \tag{4}$$

In order to obtain the maximum value of γ, we need to optimally design the phase shift of each element. Following the method in [15], by setting the phases $\phi_i = \vartheta_i + \varphi_i$, the maximum γ can be obtained as

$$\gamma = \frac{A^2\bar{\gamma}}{d_s^2 d_r^2}, \tag{5}$$

where $A = \sum_{i=1}^{N} \alpha_i\beta_i$. Moreover, the average SNR can be written by $\bar{\gamma} = \frac{P_s G_s G_r (uw\cos(\theta_i^e))^2}{16\pi^2\sigma_n^2}$. It intuitively shows that the large size of the RIS can bring large average SNR where the term of $uw\cos(\theta_i^e)$ represents the total effective area of the beam on the RIS as seen from the source.

III. SNR Coverage Probability Analysis

In the section, we give the detailed process of deriving the SNR coverage probability. Technically, we first determine the distribution of A^2 for $N = 1$ and $N \geq 1$. Then, the SNR coverage probability can be obtained with the aid of the cumulative distribution function (CDF) of A^2.

A. Deriving the Exact SNR Coverage Probability for $N = 1$

We first provide the PDF of $\alpha\beta$, and then derive its CDF.

Lemma 1. *For two i.i.d. Rayleigh RVs α and β with fading coefficients of σ_1 and σ_2, respectively, the PDF of $\eta = \alpha\beta$ can be expressed as*

$$f_\eta(\eta) = \frac{\eta}{a^2}\mathcal{K}_0\left(\frac{\eta}{a}\right), \tag{6}$$

where $a = \sigma_1\sigma_2$ and $\mathcal{K}_0(\cdot)$ is the zeroth order of modified Bessel function of the second kind.

Proof: The readers can refer to [23] for the detailed derivation of the distribution of the product of two i.i.d. Rayleigh RVs based on Meijer's G-function. ■

Lemma 2. *For N=1, the CDF of η can be obtained as*

$$F_\eta(\eta) = 1 - \frac{\eta}{a}\mathcal{K}_1(\frac{\eta}{a}), \tag{7}$$

where $\mathcal{K}_1(\cdot)$ is the first order of modified Bessel function of the second kind.

Proof: See Appendix A.

We can further obtain the CDF of η^2 by $F_{\eta^2}(\eta) = F_\eta(\sqrt{\eta})$. Then, we can derive the exact SNR coverage probability for $N = 1$.

Theorem 1. *For $N = 1$ and specific SNR threshold γ_{th}, the exact SNR coverage probability can be represented as*

$$P_{\text{cov}}(\gamma_{\text{th}}) = \frac{d_s d_r}{\sigma_1\sigma_2}\sqrt{\frac{\gamma_{\text{th}}}{\bar{\gamma}}}\mathcal{K}_1\left(\frac{d_s d_r}{\sigma_1\sigma_2}\sqrt{\frac{\gamma_{\text{th}}}{\bar{\gamma}}}\right). \tag{8}$$

Proof: The SNR coverage probability is defined as the probability that the SNR is large than a specific threshold, which can be expressed as

$$\begin{aligned} P_{\text{cov}}(\gamma_{\text{th}}) &= Pr(\gamma \geq \gamma_{\text{th}}) = 1 - Pr(\gamma \leq \gamma_{\text{th}}), \\ &= 1 - F_{\eta^2}\left(\frac{\gamma_{\text{th}}}{\bar{\gamma}} d_s^2 d_r^2\right). \end{aligned} \tag{9}$$

We can obtain (8) by combining (7) and (9). ■

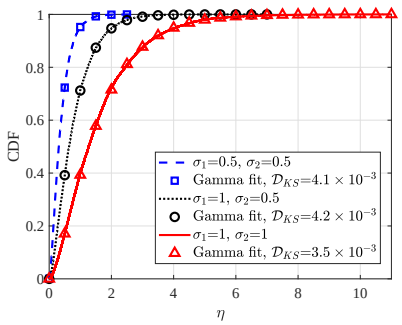

Fig. 2. Actual CDFs of η with Gamma fits for different fading coefficients.

B. Approximating SNR Coverage Probability for Arbitrary N

The derivation becomes more complicated and intractable for N>1. In practice, the distribution of η is in accordance with K-distribution $K(b,\nu)$ with $b = a = \sigma_1\sigma_2$ and $\nu = 0$ [25]. Due to the complexity and intractability of K-distribution, we use the Gamma distribution to approximate it, for the following reasons: (i) The Gamma distribution is a Type-III Pearson distribution that is widely used in fitting the distributions for positive RVs [26]. (ii) It is known that A is the sum of K-distributed η_i. Leveraging by the additive characteristic of Gamma distribution, the distribution of A can be readily obtained for the case of multiple elements [27].

Lemma 3. *With the method of moment matching, the distribution of η can be approximated as Gamma distribution,*

$$\eta \sim Ga(\frac{\pi^2}{16-\pi^2}, \frac{16-\pi^2}{2\pi}\sigma_1\sigma_2), \tag{10}$$

where $Ga(k,\theta)$ represents Gamma distribution, in which $\theta = \frac{16-\pi^2}{2\pi}\sigma_1\sigma_2$ is the scale parameter, $k = \frac{\pi^2}{16-\pi^2}$ is the shape parameter, and $\Gamma(\cdot)$ is the Gamma function.

Proof: See Appendix B.

The Kolmogorov-Smirnov (KS) test is widely used to examine the fitting goodness between two distributions, enabling us to assess the accuracy of approximation using the statistic $\mathcal{D}_{KS}$ that is defined as the maximum divergence of two CDFs,

$$\mathcal{D}_{KS} = \max|F_{\text{Approx}}(t) - F_{\text{Actual}}(t)|. \tag{11}$$

As shown in Fig. 2, the Gamma distribution in (10) is used to fit the actual CDFs of η. The results show perfect agreements between them for different σ_1 and σ_2. The small $\mathcal{D}_{KS}$ with an order of magnitude around 10^{-3} confirms the high accuracy of the Gamma approximation.

According to the addictive characteristic of Gamma distribution, we can obtain that $A \sim Ga(Nk,\theta)$ for N elements in the RIS. Based on the CLT method in [29], [30], the results show that $A \sim \mathcal{CN}\left(\frac{N\pi}{2}a, 4N\left(1-\frac{\pi^2}{16}\right)a^2\right)$ for a large N where $a = \sigma_1\sigma_2$. For simplicity, we assume σ_1=σ_2=1, a comparison between our proposed Gamma approximation and CLT-based Gaussian approximation is shown in Fig. 3. The actual PDFs of A are generalized by 10^5 independent channel realizations. The smaller $\mathcal{D}_{KS}$ confirms that Gamma distributions for different N better match with actual PDFs than Gaussian distributions. For the Gaussian fit, there is a certain discrepancy with the actual PDF, especially for small

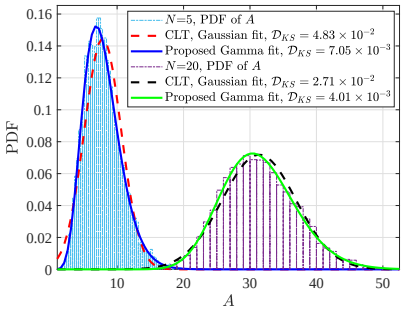

Fig. 3. Comparison of proposed Gamma and CLT-based Gaussian fitting.

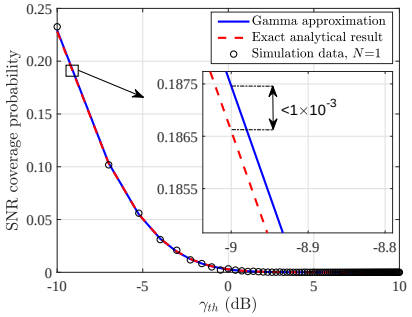

Fig. 4. Results of the exact analysis, Gamma approximation, and simulation.

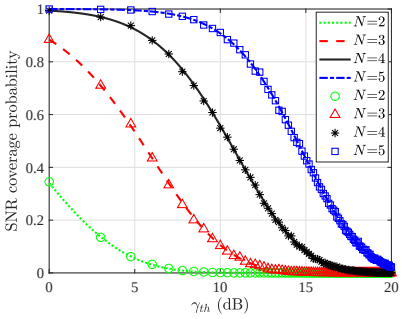

Fig. 5. Results of Gamma approximations (lines) and simulations (markers).

N. However, Fig. 3 shows that the difference between actual PDF and Gaussian fit reduces with N increasing from 5 to 20. Thus, the Gaussian distribution can apply to a large number of surfaces (several dozens or more) for realizing an insignificant discrepancy, whereas the Gamma distribution is more general without the limitation in the number of surfaces.

Correspondingly, we can obtain that A^2 follows a generalized Gamma distribution with parameters of $p = \frac{1}{2}$, $d = \frac{Nk}{2}$, and $q = \theta^2$ [31], whose CDF is expressed as

$$F_{A^2}\left(z, \frac{1}{2}, \frac{Nk}{2}, \theta^2\right) = \frac{\zeta(Nk, \frac{\sqrt{z}}{\theta})}{\Gamma(Nk)}, \tag{12}$$

where $\zeta(\cdot,\cdot)$ denotes the lower incomplete Gamma function.

Theorem 2. *For arbitrary N, given the threshold γ_{th}, the general form of SNR coverage probability is expressed as*

$$P_{\text{cov}}(\gamma_{\text{th}}) = \frac{\Gamma(Nk, s)}{\Gamma(Nk)}, \tag{13}$$

where $s = \frac{d_s d_r}{\theta}\left(\frac{\gamma_{th}}{\bar{\gamma}}\right)^{\frac{1}{2}}$ and $\Gamma(\cdot,\cdot)$ is the upper incomplete Gamma function.

Proof: Same as the proof of Theorem 1, the SNR coverage probability is expressed as

$$\begin{aligned} P_{\text{cov}}(\gamma_{\text{th}}) &= 1 - F_{A^2}\left(\frac{\gamma_{\text{th}}}{\bar{\gamma}} d_s^2 d_r^2\right), \\ &= 1 - \frac{\zeta\left(Nk, \frac{2\pi d_s d_r}{(16-\pi^2)\sigma_1\sigma_2}\left(\frac{\gamma_{\text{th}}}{\bar{\gamma}}\right)^{\frac{1}{2}}\right)}{\Gamma(Nk)}. \end{aligned} \tag{14}$$

where the $\zeta(\cdot,\cdot)$ can be calculated by

$$\zeta(Nk, s) = \Gamma(Nk) - \Gamma(Nk, s). \tag{15}$$

Substituting (15) into (14), Theorem 2 can be proved. ■

For intuitively validating and interpreting the derived result, we show the following remarks for the *asymptotic analysis*.

Remark 1. From the perspective of SNR threshold, it can be obtained that $P_{\text{cov}}^{s=0} = 1$ when $\gamma_{\text{th}} = 0$ since $\Gamma(Nk) = \Gamma(Nk, 0)$ always holds. Moreover, we have $P_{\text{cov}}^{s\to\infty} = 0$ when $\gamma_{\text{th}} \to \infty$ since $\Gamma(Nk) = \zeta(Nk, \infty)$ always holds.

Remark 2. From the perspective of the number of elements, since $Q(Nk, s) = \Gamma(Nk, s)/\Gamma(Nk)$ represents the CDF of Poisson distribution with parameter s, it directly has $Pr(X < 0) = 0$ and $Pr(X < \infty) = 1$ for positive Poisson distributed RV X, which are equivalent to the cases of $N = 0$ and $N \to \infty$, respectively. Thus, we can obtain that $P_{\text{cov}}^{N=0} = 0$ and $P_{\text{cov}}^{N\to\infty} = 1$, corresponding to two limits of no element and infinite elements, respectively. The analyses verify the rationality of derived expression.

C. Finding the Optimal Number of Elements for RIS

It has shown that the complete SNR coverage probability ($P_{\text{cov}} = 1$) achieves when N is infinite. Practically, for a specific communication scenario with a fixed SNR requirement, the complete coverage can be guaranteed when N reaches a certain number or above. Thus, it is critical to determine the optimal (*minimum*) number, which can significantly reduce the cost of deployment. Fortunately, we can find the optimal N^* by solving the equation of $\Gamma(Nk, s) = \Gamma(Nk)$ based on (13) with the numerical method, given by

$$N^* = \min\{N | \Gamma(Nk, s) = \Gamma(Nk)\},\ N \in \mathbb{N}. \tag{16}$$

IV. Simulation Results

In this section, we present simulation results to verify the derived expressions and investigate the impacts of many factors on the SNR coverage probability. The parameters are set as f_c= 30 GHz, P_s= 1 mW, G_s=G_r= 0 dBi, d_s=d_r= 100 m, σ_n^2= -90 dBm, and $uw = Nl_e^2$ where l_e is the side length of the square element. Note that remaining parameters may change for different purposes and simulation results are obtained by averaging over 10^5 independent channel realizations.

We first carry out a comparison among the exact analysis, Gamma approximation, and simulation for $N = 1$, shown in Fig. 4. It is seen that both the exact result and Gamma approximation are perfectly consistent with the simulation result,

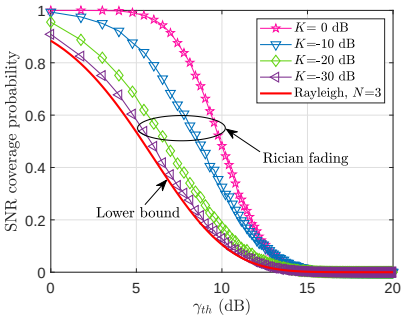

Fig. 6. SNR coverage probability under Rayleigh *vs.* Rician fading.

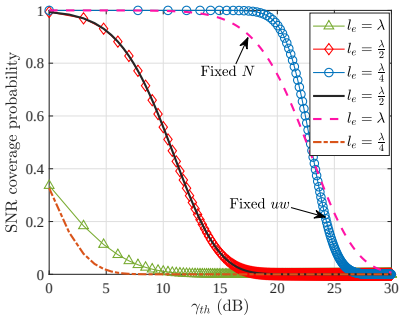

Fig. 8. SNR coverage probability *vs.* different sizes of elements.

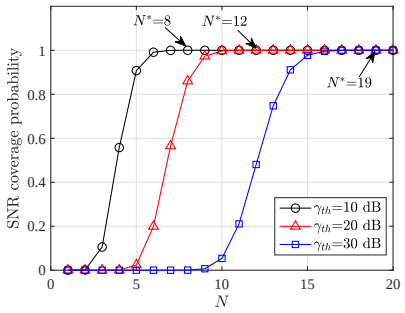

Fig. 7. SNR coverage probability *vs.* N for different SNR thresholds.

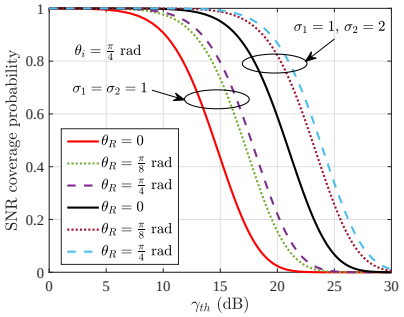

Fig. 9. SNR coverage probability *vs.* fading coefficients and incident angles.

which reveals the correctness of our derivations. The difference between the exact analysis and Gamma approximation is also illustrated in Fig. 4, which shows that the difference is smaller than 10^{-3} for the SNR threshold of -9 dB, further indicating the high accuracy of the Gamma approximation.

For $N>1$, we compare the simulated result with the Gamma approximation, as shown in Fig. 5. The results turn out perfect matching for different N. It is also found that the SNR coverage probability can be greatly improved by increasing N. As an example, with γ_{th}=10 dB, the probability raises 0.45 by increasing N from 3 to 4. Furthermore, we compare the difference between Rayleigh and Rician fading [32]. Fig. 6 shows the SNR coverage probabilities for different Rician *K*-factors in dB and Rayleigh fading when $N = 3$. It is seen that the larger *K*-factor gives rise to a higher probability. Moreover, the result under Rayleigh fading is the lower bound of the SNR coverage probability under Rician fading since Rayleigh fading can be regarded as the Rician fading with $K = 0$ ($-\infty$ dB). Since analytical results can always perfectly match with simulations, we only use the analytical result in the sequel.

To find the optimal number of surfaces, we illustrate the SNR coverage probability versus N, shown in Fig. 7. Results indicate that the full coverage can be achieved for different SNR thresholds when N reaches a certain number (l_e is fixed as $\lambda/2$). More specifically, the optimal number (N^*) is 8, 12, and 19 for SNR thresholds of 10 dB, 20 dB, and 30 dB, respectively. Notably, the optimal numbers based on the analysis are the same as the numerical results in (16).

We investigate the impact of the size (l_e) of the element in Fig. 8. We consider two conditions consisting of fixed N and fixed uw, respectively. For fixed N (= 4), the lines without markers show that larger size of element leads to a higher SNR coverage probability since the total area of the RIS becomes larger. For fixed uw (curves with markers), the smaller size results in a higher probability since N (= 1, 4, 16) increases.

The influences of channel fading coefficients and effective incident angles are investigated in Fig. 9. Results show that the larger coefficient led by severe fading contributes to a higher SNR coverage probability, thanks to the constructive superposition of incoming waves. For effective incident angles (θ_i^e), Fig. 9 shows that smaller angles cause larger probabilities since the term of $\cos(\theta_i^e)$ measures the effective impinging area of the incident wave. It is found that the upper bound corresponds to the situation when $\theta_i = \theta_R$ exists. The result provides an insight to the better placement of the RIS plane.

V. Conclusion

In this work, we comprehensively analyzed the SNR coverage probability of RIS-aided communication systems. We derived the closed-form SNR coverage probability for $N = 1$. With Gamma approximation, we obtained a more general expression of SNR coverage probability for an arbitrary number of N. We investigated the impacts of many factors on the SNR coverage probability. We found that the larger number or area of the RIS can significantly improve the performance with controllable variables, including N, l_e, θ_i, and θ_R. Moreover, owing to the constructive superposition of impinging waves, the uncontrollable channel fading coefficients are also beneficial to increasing SNR coverage probability. The work not only derived a general form of SNR coverage probability but also provided many useful insights for the deployment of RIS.

APPENDIX A
PROOF OF LEMMA 2

The CDF of η can be obtained based on (6),

$$\begin{aligned} F_\eta(\eta) &= \int_{-\infty}^{\eta} f_\eta(x)dx = \int_0^{\eta} \frac{x}{a^2}\mathcal{K}_0\left(\frac{x}{a}\right)dx, \\ &= \lim_{x\to 0}\frac{x}{a}\mathcal{K}_1\left(\frac{x}{a}\right) - \frac{\eta}{a}\mathcal{K}_1(\frac{\eta}{a}). \end{aligned} \tag{A.1}$$

By using the l'Hôpital's rule, we can seek the limit, given by

$$\lim_{x\to 0}\frac{x}{a}\mathcal{K}_1\left(\frac{x}{a}\right) = \lim_{x\to 0}\frac{\frac{-(\mathcal{K}_0(\frac{x}{a})+\mathcal{K}_2(\frac{x}{a}))}{2a}}{-\frac{a}{x^2}}. \tag{A.2}$$

With [14, Eq. 8.446], when $x \to 0$, the series expansion is

$$-\frac{\mathcal{K}_0(\frac{x}{a})+\mathcal{K}_2(\frac{x}{a})}{2a} \to -\frac{a}{x^2} + \frac{2\log(\frac{1}{2a}) + 2\log(x) + 2\epsilon + 1}{4a}. \tag{A.3}$$

By combining (A.1)-(A.3), we can have Lemma 2.

APPENDIX B
PROOF OF LEMMA 3

We first calculate the n-th moment of Gamma distribution, expressed as [28],

$$\mu_n^G = \theta^n \prod_{i=1}^{n}(k+i-1). \tag{B.1}$$

while the moment of distribution of η can be obtained with the aid of $\mathcal{K}_0(x/a) = \int_0^\infty \frac{\cos(xt/a)}{\sqrt{t^2+1}}dt$, given by

$$\mu_n^\eta = \int_0^\infty \int_0^\infty \frac{x^{n+1}}{a^2}\frac{\cos(\frac{xt}{a})}{\sqrt{t^2+1}}dtdx. \tag{B.2}$$

By matching the first and second moments, i.e., $\mu_1^\eta = \frac{a\pi}{2} = k\theta = \mu_1^G$ and $\mu_2^\eta = 4a^2 = k(k+1)\theta^2 = \mu_2^G$, the results of k and θ can be obtained and one can have Lemma 3.

REFERENCES

[1] J. Zhang, E. Björnson, M. Matthaiou, D. W. K. Ng, H. Yang, and D. J. Love, "Prospective multiple antenna technologies for beyond 5G," *IEEE J. Sel. Areas Commun.*, vol. 38, no. 8, pp. 1637-1660, Aug. 2020.

[2] M. Nemati, J. Park, and J. Choi, "RIS-assisted coverage enhancement in millimeter-wave cellular networks," *IEEE Access*, vol. 8, pp. 188171-188185, Oct. 2020.

[3] M. Cui, G. Zhang, and R. Zhang, "Secure wireless communication via intelligent reflecting surface," *IEEE Wireless Commun. Lett.*, vol. 8, no. 5, pp. 1410-1414, Oct. 2019.

[4] C. Huang, A. Zappone, G. C. Alexandropoulos, M. Debbah, and C. Yuen, "Reconfigurable intelligent surfaces for energy efficiency in wireless communication," *IEEE Trans. Wireless Commun.*, vol. 18, no. 8, pp. 4157-4170, Aug. 2019.

[5] C. Huang, G. C. Alexandropoulos, A. Zappone, M. Debbah, and C. Yuen, "Energy efficient multi-user MISO communication using low resolution large intelligent surfaces," in *Proc. IEEE Globecom Workshops (GC Wkshps)*, Abu Dhabi, United Arab Emirates, 2018, pp. 1-6.

[6] C. Huang *et al.*, "Holographic MIMO surfaces for 6G wireless networks: opportunities, challenges, and trends," *IEEE Wireless Commun.*, vol. 27, no. 5, pp. 118-125, Oct. 2020.

[7] Z. Wan, Z. Gao, M. Renzo, and M. Alouini, "Terahertz massive MIMO with holographic reconfigurable intelligent surfaces," *arXiv:2009.10963*, 2020, [online] Available: https://arxiv.org/pdf/2009.10963.

[8] C. Huang, Z. Yang, G. C. Alexandropoulos, K. Xiong, L. Wei, C. Yuen, and Z. Zhang, "Hybrid beamforming for RIS-empowered multi-hop terahertz communications: a DRL-based method," *IEEE J. Sel. Areas Commun.*, 2021, to appear. [online] Available: https://arxiv.org/abs/2009.09380.

[9] Q. Wu and R. Zhang, "Intelligent reflecting surface enhanced wireless network via joint active and passive beamforming," *IEEE Trans. Wireless Commun.*, vol. 18, no. 11, pp. 5394-5409, Aug. 2019.

[10] Q. Tao, J. Wang, and C. Zhong, "Performance analysis of intelligent reflecting surface aided communication systems," *IEEE Commun. Lett.*, vol. 24, no. 11, pp. 2464-2468, Nov. 2020.

[11] D. Kudathanthirige, D. Gunasinghe, and G. Amarasuriya, "Performance analysis of intelligent reflective surfaces for wireless communication," *arXiv:2002.05603*, 2020, [online] Available: http://arxiv.org/abs/2002.05603.

[12] Y. Jia, C. Ye, and Y. Cui, "Analysis and optimization of an intelligent reflecting surface-assisted system with interference," *arXiv:2002.00168*, 2020, [online] Available: http://arxiv.org/abs/2002.00168.

[13] M. Badiu and J. P. Coon, "Communication through a large reflecting surface with phase errors," *IEEE Wireless Commun. Lett.*, vol. 9, no. 2, pp. 184-188, Feb. 2020.

[14] W. Zhao, G. Wang, S. Atapattu, T. A. Tsiftsis, and X. Ma, "Performance analysis of large intelligent surface aided backscatter communication systems," *IEEE Wireless Commun. Lett.*, vol. 9, no. 7, pp. 962-966, Jul. 2020.

[15] L. Yang, Y. Yang, M. O. Hasna, and M. S. Alouini, "Coverage, probability of SNR gain, and DOR analysis of RIS-aided communication systems," *IEEE Wireless Commun. Lett.*, vol. 9, no. 8, pp. 1268-1272, Aug. 2020.

[16] E. Basar, M. Di Renzo, J. De Rosny, M. Debbah, M. S. Alouini, and R. Zhang, "Wireless communications through reconfigurable intelligent surfaces," *IEEE Access*, vol. 7, pp. 116753-116773, 2019.

[17] T. Van Chien, L. T. Tu, S. Chatzinotas, and B. Ottersten, "Coverage probability and ergodic capacity of intelligent reflecting surface-enhanced communication systems," *IEEE Commun. Lett.*, vol. 25, no. 1, pp. 69-73, Jan. 2021.

[18] H. Ibrahim, H. Tabassum, and U. T. Nguyen, "Exact coverage analysis of intelligent reflecting surfaces with Nakagami-m channels," *IEEE Trans. Veh. Technol.*, Early Access, Jan. 2021, doi: 10.1109/TVT.2021.3050046.

[19] J. C. B. Garcia, A. Sibille, and M. Kamoun, "Reconfigurable intelligent surfaces: bridging the gap between scattering and reflection," *IEEE J. Sel. Areas Commun.*, vol. 38, no. 11, pp. 2538-2547, Nov. 2020.

[20] S. Abeywickrama, R. Zhang, Q. Wu, and C. Yuen, "Intelligent reflecting surface: practical phase shift model and beamforming optimization," *IEEE Trans. Commun.*, vol. 68, no. 9, pp. 5849-5863, Sept. 2020.

[21] W. Tang *et al.*, "Wireless communications with reconfigurable intelligent surface: path loss modeling and experimental measurement," *IEEE Trans. Wireless Commun.*, vol. 20, no. 1, pp. 421-439, Jan. 2021.

[22] Ö. Özdogan, E. Björnson, and E. G. Larsson, "Intelligent reflecting surfaces: physics, propagation, and pathloss modeling," *IEEE Wireless Commun. Lett.*, vol. 9, no. 5, pp. 581-585, May 2020.

[23] J. Salo, H. M. El-Sallabi, and P. Vainikainen, "The distribution of the product of independent Rayleigh random variables," *IEEE Trans. Antennas Propag.*, vol. 54, no. 2, pp. 639-643, Feb. 2006.

[24] I. S. Gradshteyn and I. M. Ryzhik, *Table of Integrals, Series and Products*, 7th ed. Academic Press Inc, 2007.

[25] E. Jakeman and P. N. Pusey, "Significance of K distributions in scattering experiments," *Phys. Rev. Lett.*, 40, 546-550, Feb. 1978.

[26] S. Al-Ahmadi and H. Yanikomeroglu, "On the approximation of the generalized-K distribution by a gamma distribution for modeling composite fading channels," *IEEE Trans. Wireless Commun.*, vol. 9, no. 2, pp. 706-713, Feb. 2010.

[27] S. Atapattu, C. Tellambura, and H. Jiang, "A mixture gamma distribution to model the SNR of wireless channels," *IEEE Trans. Wireless Commun.*, vol. 10, no. 12, pp. 4193-4203, Dec. 2011.

[28] S. Atapattu, R. Fan, P. Dharmawansa, G. Wang, J. Evans, and T. A. Tsiftsis, "Reconfigurable intelligent surface assisted two-way communications: performance analysis and optimization," *IEEE Trans. Commun.*, vol. 68, no. 10, pp. 6552-6567, Oct. 2020.

[29] Z. Yang, W. Xu, C. Huang, J. Shi, and M. Shikh-Bahaei, "Beamforming design for multiuser transmission through reconfigurable intelligent surface," *IEEE Trans. Commun.*, Early Access, 2020, doi: 10.1109/TCOMM.2020.3028309.

[30] J. Lyu and R. Zhang, "Spatial throughput characterization for intelligent reflecting surface aided multiuser system," *IEEE Wireless Commun. Lett.*, vol. 9, no. 6, pp. 834-838, Jun. 2020.

[31] P. G. Moschopoulos, "The distribution of the sum of independent gamma random variables," *Ann. Inst. Stat. Math.*, 37, 541-544, Dec. 1985.

[32] B. Di, H. Zhang, L. Song, Y. Li, Z. Han, and H. V. Poor, "Hybrid beamforming for reconfigurable intelligent surface based multi-user communications: achievable rates with limited discrete phase shifts," *IEEE J. Sel. Areas Commun.*, vol. 38, no. 8, pp. 1809-1822, Aug. 2020.